Biointerface Research in Applied Chemistry
Open-Access Journal (ISSN: 2069-5837)

Article
Volume 13, Issue 4, 2023, 253
https://doi.org/10.33263/BRIAC133.253

Numerical Simulation of p-i-n GaAs Photovoltaic Cell Using SCAPS-1D

Mohammed Azza [1], El Hadi Chahid [1,2], Abdellatif Hmairrou [1], Rachid Abdia [2], Malika Tridane [1], Abdessamad Malaoui [2], Said Belaaouad [1]

[1] Laboratory of Physical Chemistry of Materials, Faculty of Sciences Ben M'sik, Hassan II University of Casablanca, Morocco
[2] Research Laboratory in Physics and Sciences for Engineers (LRPSI), Polydisciplinary Faculty, Sultan Moulay Slimane University, Beni Mellal, Morocco
* Correspondence: mohammedazza81@gmail.com (M.A.);

Received: 24.03.2022; Accepted: 29.04.2022; Published: 10.06.2022

Abstract: The operation of solar cells based on GaAs p-i-n GaAs is investigated via numerical simulation using "SCAPS-1D. This involves optimizing certain physical and geometric parameters of these cells to increase their performance under standard conditions. The simulation was carried out on a "p-i-n" solar cell based on GaAs by studying several parameters, namely; the effect of the thickness of each layer of the PV cell, the impact of doping on the values of the open-circuit voltage (Voc) and short-circuit current density (Jsc), as well as conversion efficiency and fill factor (FF). The obtained results show that the behavior of the solar cells studied is directly related to the temperature and to the thickness of the intrinsic layers. In fact, the optimal parameters for high performance are: Voc= 0.85 V, Jsc= 24.52 mA/cm^2, FF= 85,70 % and η=21.05 %.

Keywords: photovoltaic cells; SCAPS-1D; gallium arsenide; efficiency; numerical simulation.

1. Introduction

The use of renewable energies to generate electricity is one of the solutions developed to face the decrease in natural resources[1]. Increase the energy independence of countries and reduce the anthropic impact on the environment [2, 3]. The solar energy arriving on Earth at each moment is gigantic and can be converted into electricity using photovoltaic cells [4]; the basic solar cell is a semiconductor PN junction whose efficiency depends on the absorbed photons and the electron-hole pairs generated in the space charge region [5, 6]. One of the possibilities to improve this absorption is to intercalate an intrinsic layer between the P-doped and N-doped layers [7-9], which gives a solar cell based on a p-i-n structure [10, 11]. Many works were done in our laboratory in order to find new organic and inorganic condensed phosphates used for photovoltaic cells [12-21].

Most solar cells are based on a PN junction; in thin-film solar cells [22-24], the diffusion lengths are usually very small; in fact, they are often less than the thickness of the solar cell [25, 26]. Therefore, diffusion alone is not sufficient to ensure the transport and collection of photo-generated carriers [27, 28]. Therefore, the internal electric field is also used to support the photo-generated carriers' transport [29]. This is only possible with the p-i-n structure: the internal electric field extends over the entire i-layer and governs the photo-generated carriers' transport and separation [30, 31]. Our research will therefore focus on studying heterojunction

and p-i-n solar cells by simulating the behavior of these solar cells using the SCAPS simulation software. In particular, the optimization of geometrical and physical parameters; The first considers the effect of intrinsic layer thickness, whereas the second considers the impact of temperature on the perfillance of the GaAs and p-i-n structure cell.

2. Materials and Methods

2.1. Structure of a p-i-n solar cell.

Our work will focus on studying a solar cell with a p-i-n structure based on amorphous silicon. It will essentially be the simulation of the behavior of this solar cell using the SCAPS simulation software [32].

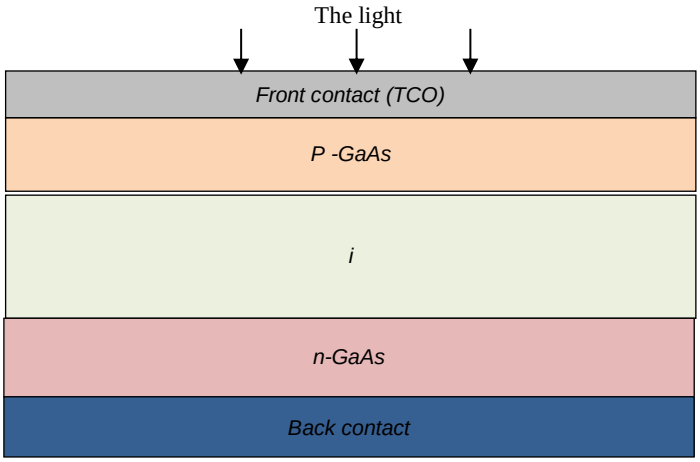

Figure 1. The structure of the p-i-n solar cell.

Figure 1 illustrates the cell's structure which was used in the simulation A glass panel, a transparent conductive oxide (TCO) anode, a p-i-n junction make up the structure, and an Al cathode. The parameters used for the gallium arsenic p-i-n solar cell at T=300 K are in the following Table 1.

Table 1. Parameters used to simulate the gallium arsenide p-i-n solar cell [33].

Parameters	p-layer	i- layer	n- layer
Thickness (nm)	9	500	20
$\boldsymbol{\varepsilon_r}$	12.4	12.4	12.4
$\boldsymbol{\chi_e(eV)}$	4.07	4.07	4.07
$\boldsymbol{E_g(eV)}$	1.42	1.42	1.42
$\boldsymbol{\mu_n(cm^2.V^{-1}.s^{-1})}$	8500	8500	8500
$\boldsymbol{\mu_p(cm^2.V^{-1}.s^{-1})}$	400	400	400
$\boldsymbol{N_C(cm^{-3})}$	4.7×10^{17}	4.7×10^{17}	4.7×10^{17}
$\boldsymbol{N_V(cm^{-3})}$	7×10^{18}	7×10^{18}	7×10^{18}
$\boldsymbol{N_A(cm^{-3})}$	10^{17}	0	0
$\boldsymbol{N_D(cm^{-3})}$	0	0	10^{17}

2.2. Operating principle of a p-i-n solar cell.

The operating principle of a photovoltaic solar cell is illustrated in Figure 2, which represents the function of a PN junction where the space charge zone. The incident photons create carriers in each of the regions p, i, n, and their behavior differs depending on the region of the junction where they are created.

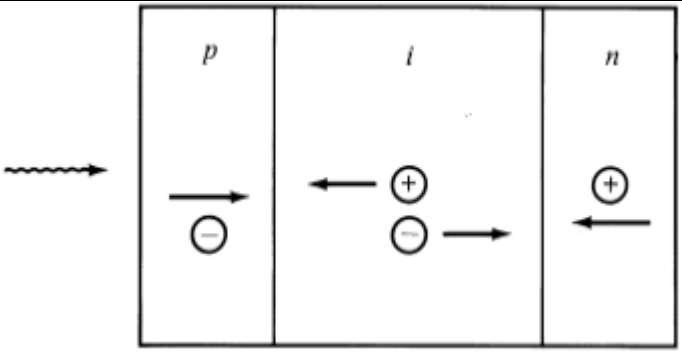

Figure 2. Operating principle of a solar cell with a p-i-n structure.

2.2.1. For *p* and *n*-regions.

In these layers regions, the minority photo-carriers diffuse. Those that reach the space charge region are propelled by the electric field, directed from the positively charged part to the negatively charged part (Figure 2), to the region where they become the majority. There is thus separation of the carriers in the ZCE towards the p and n regions [34, 35]. These photo-carriers contribute to the current by their diffusion; they create a photo-current of diffusion.

2.2.2. For intrinsic layer.

The electric field dissociates the electron-hole pairs created by the photons; the electron is propelled towards the n-type region and the hole towards the p-type region. These carriers give rise to a photo-current of generation [36].

2.3. Electrical parameters of a solar cell.

We often talk about the conversion efficiency of photovoltaic cells; this term corresponds to the cell's capacity to transfill the energy of the photons that hit it. These measurements are now standardized [37]. Therefore, the manufacturers test the solar cells under an artificial light spectrum corresponding to a typical solar spectrum AM1.5 (the total irradiance received on the Earth's surface at an altitude of 0° with an angle of 48°) under a fixed temperature at 25°C [38]. For simplicity, this convention has been used to normalize the efficiency given in the collector manuals in order to compare them. The average total power received during the tests by the cells assembled in PV module is 1000W/m² under 25°C [39]. A number of scientists are working to increase solar cells' power density [40]. Currently, the commercial panels have most of them, an efficiency of about 14% [41]. This can result in the production of 140 Watts for a PV module that receives 1000 W/m^2. Research into the materials that make up the cells is in full swing, as is research into optimizing the manufacture of PV cells and panels. An important parameter is often used from the current-voltage I (V) characteristic to qualify the quality of a PV cell or the quality of a cell or a PV generator: the fill factor (FF). This coefficient represents the ratio between the maximum power that the cell can deliver P_{max} and the power-filled by the rectangle I_{CC}. V_{oc} [42].

$$FF = \frac{P_{max}}{I_{CC}.V_{oc}}$$

As the value of this factor increases, so does the exploitable power. The best cells will have been subject to technological compromises to achieve the ideal characteristics possible. The efficiency of a cell can be written [43]:

$$\eta = \frac{P_{max}}{P_{inc}}$$

where $P_{max} = V_{max}.I_{max}$ and $P_{inc} = 1000\ W/m^2$.

2.4. The crystal structure of GaAs.

In this section, we have used Vesta software to represent the GaAs crystal structure, illustrated in figure 3, and the X-ray diffraction spectrum shown in figure 4 [44]. The GaAs structure crystallizes in two face-centered sublattices, one is formed of element III, and the other is formed of element V [45-47]. At the nanometric scale, the wurtzite structure also becomes stable for some III-V materials (GaAs, InAs). It offers another possibility to tune their optoelectronic properties when this transition is well-controlled [48, 49]. Several studies have shown that nanowires or quantum boxes can control this transition. Gallium arsenic is a compound with the molecular formula GaAs, a member of the III-V semiconductors group. In particular, it is a semiconductor material used for the realization of electroluminescent diodes in microwaves and optoelectronic components, infrared or photovoltaic cells. GaAs is called "III-V" because gallium and arsenic are present in columns III and V of the periodic table and therefore have three and five valence electrons [50].

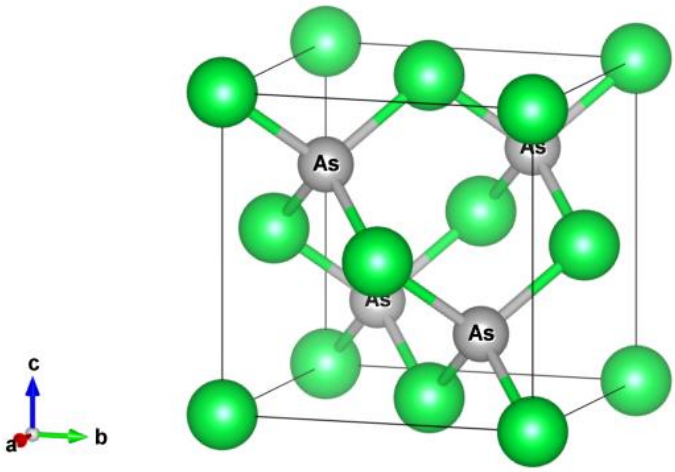

Figure 3. Zinc blende crystal structure of GaAs.

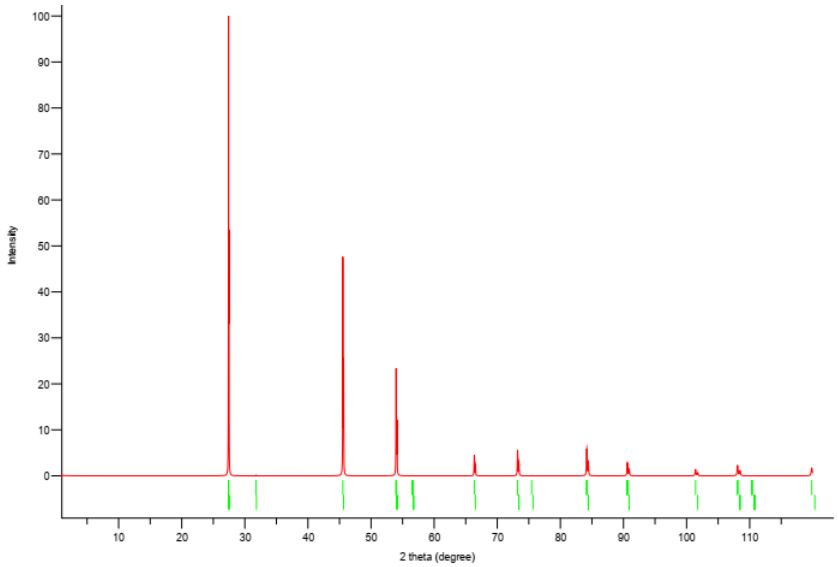

Figure 4. X-ray diffraction spectrum of the GaAs structure.

3. Results and Discussion

The parameters used for the p-i-n solar cell based on amorphous silicon at T=300 K are listed in the table. The parameter value of the GaAs structure mesh is equal to 5.6533 Å [51]. The simulation results of GaAs solar cell junction types using SCAPS-1D are resumed in Table 2 and Figure 5. Throughout the simulation, the standard solar cell conditions are AM1.5, a temperature of 25 °C, and irradiance of 1000 W/m^2.

Table 2. Simulated parameters of the GaAs solar cell as a function of the junction type**.**

Junction type	Material type	V_{oc}(V)	J_{cc}(mA/cm^2)	FF(%)	η(%)
p-n junction	GaAs	0.968	17.3953	85.7054	18.04
p-i-n junction	GaAs	0.8587	24.5220	85.7054	24.53

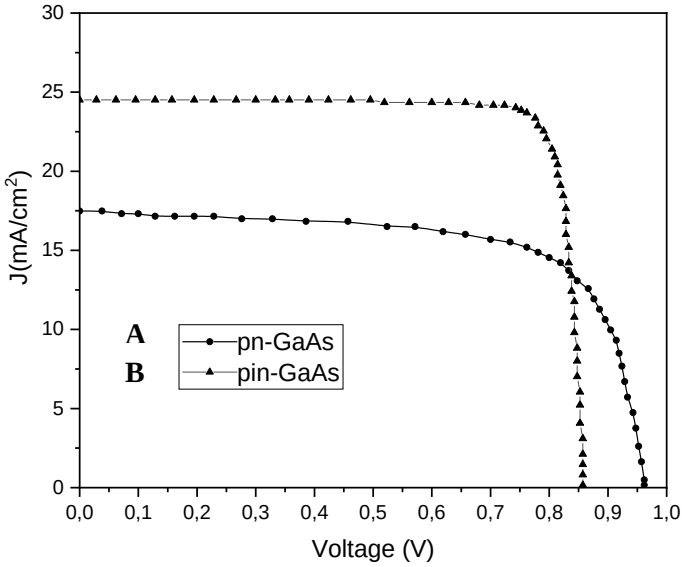

A

Figure 5. J-V characteristic of the GaAs solar cell: (**A**) the p-n junction; (**B**) the p-i-n junction.

It is observed that the use of the intrinsic layer in The short circuit current density Jsc and the open-circuit voltage Voc have both grown as a result of the GaAs p-n junction. Therefore the power conversion efficiency η has also increased. On the other hand, to ameliorate the performance of GaAs solar cell, The effect of intrinsic thickness layer and cell's temperature are studied with output parameters, which are open-circuit voltage V_{oc}, short circuit current density J_{cc}, fill factor, and conversion efficiency η.

3.1. Thickness variation of the i-layer of the p-i-n GaAs solar cell.

The obtained results are represented in Figure 6. It is noticed that V_{oc} and FF show an increase while J_{cc} increases when the thickness of the intrinsic layer increases between 400nm and 1000nm. It was found that the existence of the intrinsic layer causes an increase in cell efficiency. Indeed, This layer plays a very important role in the photovoltaic properties of the cell, in particular during the absorption phenomena.

3.2. Temperature effect.

Figure 7 represents the density current-voltage characteristic J-V as a function of different temperature values. It shows that as the temperature increases, there is a small

decrease in the short circuit current density and a large decrease in the open-circuit voltage of the solar cell.

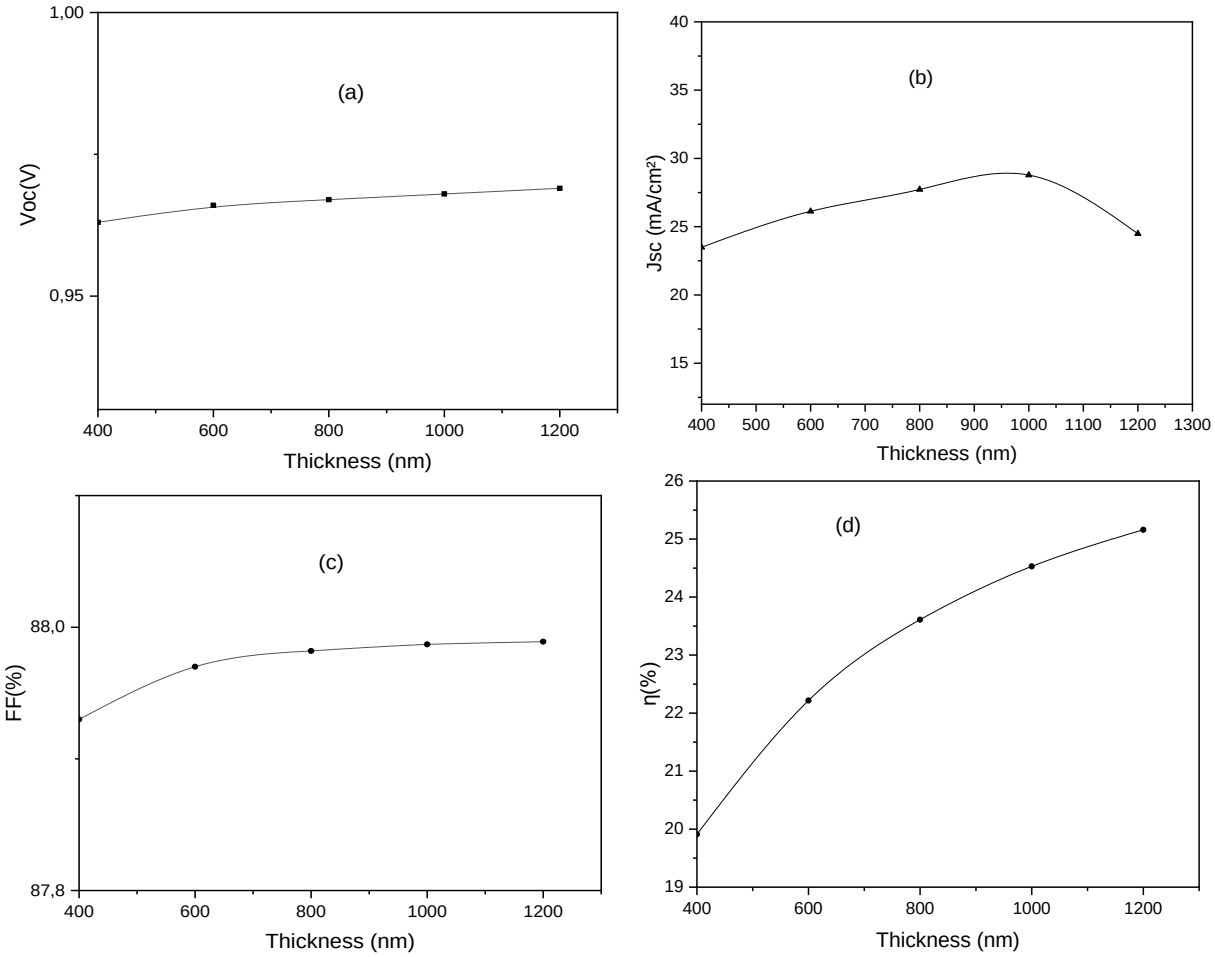

Figure 6. Effect of temperature on the J-V characteristic.

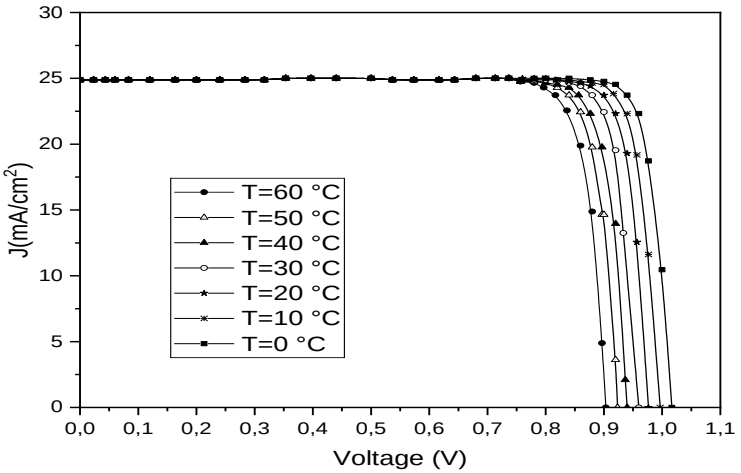

Figure 7. Effect of temperature on the J-V characteristic.

The temperature is an important parameter in the behavior of solar cells; nearly 80% is lost as heat and affects electrical and physical parameters. Indeed, we set the parameters of the p-i-n solar cell, and we change the temperature from 273 K to 323 K. Figure 8 shows the influence of temperature on V_{oc}, J_{cc}, FF, and η. It is important to note that when the temperature rises, the open-circuit voltage, efficiency, and fill factor decrease.

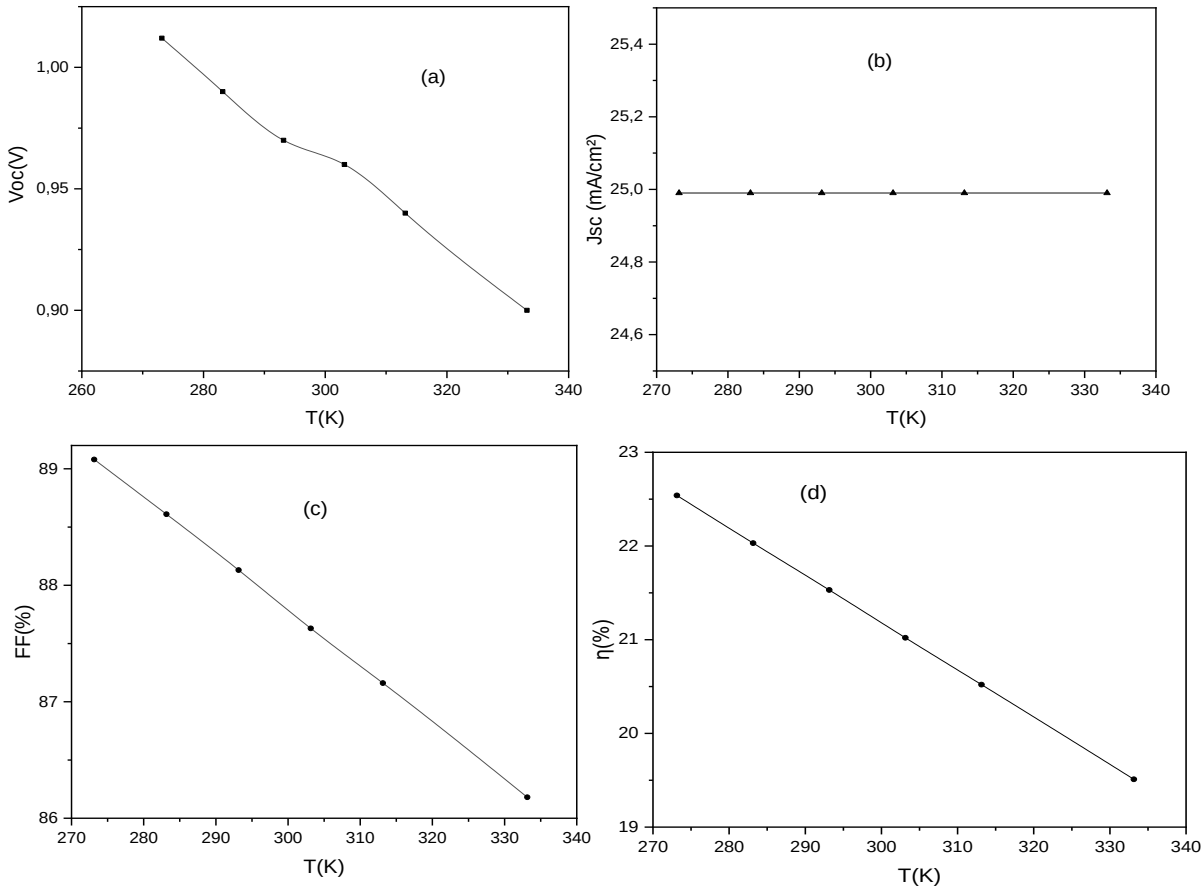

Figure 8. Effect of temperature on photovoltaic solar cells parameters.

A comparison between the simulated and experimental p-i-n solar cells is presented in Table 3. It can be concluded that the experimental and simulated values are in reasonable agreement.

Table 3. Experimental and simulation results.

Parameters	Experimental [52]	Simulation
V_{oc}(V)	0.84	0. 85
J_{cc}(mA/cm^2)	24.30	24.52
FF(%)	81.35	85.70
η(%)	20.43	21.05

4. Conclusions

In summary, we have studied the optimization of a GaAs solar cell by numerical simulation with the SCAPS-1D software. The study dealt with the influence of physical and geometrical parameters (thickness and temperature) on the efficiency of the cell and particularly on the short circuit current density J_{sc}, and open-circuit voltage V_{oc}.

The results indicate that the behavior of p-i-n solar cells is strongly related to the temperature and the geometrical parameters of the cell layers p, i, and n. On the one hand, it was found that the temperature strongly influences the value of the short circuit current density and is negligible on the open-circuit voltage when the temperature increases and, consequently, the efficiency decreases. On the other side, the intrinsic thickness of the p-i-n GaAs solar cell considerably influences the performance of the studied cell. The optimal parameters of the the p-i-n GaAs solar cell are: V_{oc}= 0.85 V, J_{sc}= 24.52 mA/cm^2, FF= 85,70% and η=21.05 %.

Funding

This research received no external funding.

Acknowledgments

The authors would like to thank Prof. Dr. Marc Burgelman, University of Gent, Belgium, for providing the SCAPS simulation software.

Conflicts of Interest

The authors declare that there is no conflict of interest regarding the publication of this paper.

References

1. Malaoui, A.; Chahid, E. Accurate calculations of the Photovoltaic cells' intrinsic parameters: The physical and electrical properties of three generations of solar cells are investigated using developed methods. *LAMBERT Academic Publishing* **2022**.
2. Milojević, M.; Nowodziński, P.;Terzić, I.; Danshina, S. Households' Energy Autonomy: Risks or Benefits for a State? *Energies* **2021**, *14*, 2026, https://doi.org/10.3390/en14072026.
3. Chou, E.; Southall, B.L.; Robards, M.; Rosenbaum, H.C. International policy, recommendations, actions and mitigation efforts of anthropogenic underwater noise. *Ocean & Coastal Management* **2021**, *202*, 105427, https://doi.org/10.1016/j.ocecoaman.2020.105427.
4. Xing, X.; Sun, F.; Qu, W.; Xin, Y.; Hong, H. Numerical simulation and experimental study of a novel hybrid system coupling photovoltaic and solar fuel for electricity generation. *Energy Conversion and Management* **2022**, *255*, 115316, https://doi.org/10.1016/j.enconman.2022.115316.
5. Feng, D.; Tervo, E.J.; Vasileska, D.; Yee, S.K.; Rohatgi, A.; Zhang, Z.M. Spatial profiles of photon chemical potential in near-field thermophotovoltaic cells. *Journal of Applied Physics* **2021**, *129*, 213101, https://doi.org/10.1063/5.0047241.
6. Pandey, R.; Madan, J.; Sharma, R. Enhanced charge extraction in metal–perovskite–metal back-contact solar cell structure through electrostatic doping: a numerical study. *IEEE Transactions on Electron Device*s **2021**, *68*, 1757-1763, https://doi.org/10.1109/TED.2021.3057029.
7. Patnaik, S.; Sahoo, D.P.; Parida, K. Recent advances in anion doped g-C3N4 photocatalysts: a review. *Carbon* **2021**, *172*, 682-711, https://doi.org/10.1016/j.carbon.2020.10.073.
8. Nam, G.H.; Sun, C.; Chung, D.S.; Kim, Y.H. Enhancing Doping Efficiency of Diketopyrrolopyrrole-Copolymers by Introducing Sparse Intramolecular Alkyl Chain Spacing. *Macromolecules* **2021**, *54*, 7870-7879, https://doi.org/10.1021/acs.macromol.1c01368.
9. Rana, M.S.; Islam, M.M.; Julkarnain, M. Enhancement in efficiency of CZTS solar cell by using CZTSe BSF layer. *Solar Energy* **2021**, *226*, 272-287, https://doi.org/10.1016/j.solener.2021.08.035.
10. Li, C.; Xu, F.; Li, Y.; Li, N.; Yu, H.; Yuanb, B.; Cao, B. An ultrahigh 84.3% fill factor for efficient CH3NH3PbI3 PiN perovskite film solar cell. *Solar Energy* **2022**, *233*, 271-277, https://doi.org/10.1016/j.solener.2022.01.035.
11. Makenali, M.; Kazeminezhad, I.; Ahmadi, V.; Roghabadi, F.A. Charge transfer balancing of planar perovskite solar cell based on a low cost and facile solution-processed CuOx as an efficient hole transporting layer. *Journal of Materials Science: Materials in Electronics* **2021**, *32*, 2312-2325, https://doi.org/10.1007/s10854-020-04996-y.
12. Kerraj, S.; Salah, M.; Chtita, S; El Idrissi, M.; Belaaouad, S.; Mohammed, M.; Komiha, N. Theoretical study of photovoltaic performances of Ru, Rh and Ir half sandwich complexes containing N, N chelating ligands in Dye-Sensitized Solar Cells (DSSCs). DFT and TD-DFT investigation. *Computational and Theoretical Chemistry* **2022**, *1209*, 113630, https://doi.org/10.1016/j.comptc.2022.113630.
13. Majdi, E.M.; Zerraf, S.; Belhabra, M.; Belaaouad, S. Chemical preparation, crystal structure and vibrational study of MnNa3P3O10. 12H2O and X-ray characterization of the new anhydrous triphosphate MnNa3P3O10. *Phase Transitions* **2022**, *95*, 50-63, https://doi.org/10.1080/01411594.2021.2009478.

14. Saouti, F.; Belaaouad, S.; Cherqaoui, A.; Naimi, Y. Polyaniline Thin Film Prepared by Electrochemical Polymerization Method. *Biointerface Research in applied chemistry* **2022**, *12*, 5523-5533, https://doi.org/10.33263/BRIAC124.55235533.
15. Majdi, E.M.; Belhabra, M.; Ouasri, A.; Fahim, I.; Essehli, R.; Belaaouad, S. Chemical Preparation, Crystal Structure Reinvestigation and Vibrational Study of CoNa3P3O10·12H2O and X-ray Characterization of the New Anhydrous Triphosphate CoNa3P3O10. *Biointerface Research in Applied Chemistry* **2021**, *12*, 2586-2602, https://doi.org/10.33263/briac122.25862602.
16. Bassam, R.; El Alouani, M.; Jabrane, M.; El Khattabi, E.H.; Tridane, M.; Belaaouad, S. Studies on the Removal of Cadmium Toxic Metal Ions by Natural Clays from Aqueous Solution by Adsorption Process. *Journal of Chemistry* **2021**, *2021*, 7873488, https://doi.org/10.1155/2021/7873488.
17. El Makhloufy, S.; Oubouaza, R.; Ouasri, A.; Belaaouad, S. X-Ray diffraction and infrared spectroscopy data review analyses of the Calcium phosphates. *Biointerface Res. Appl. Chem* **2022**, *12*, 732-755, https://doi.org/10.33263/BRIAC121.732755.
18. Oubouaza, R.; Benson, M.; Wojciechowski, J.; Chtita, S.; Tridane, M.; Belaaouad, S. Synthesis, Crystal Structure, Vibrational Study and DFT Computation of Barium Dihydrogenomonophosphate Ba (H2PO4) 2. *Biointerface Res. Appl. Chem* **2021**, *77*, C804, https://doi.org/10.33263/BRIAC121.11201133.
19. El Makhloufy, S.; Belhabra, M.; Zerraf, S.; Ouasri, A.; Chtita, S.; Saadi, M.; Belaaouad, S. Synthesis, Crystal Structure, IR spectroscopy, and DFT computation of the new variety of 2-carboxyanilinium dihydrogen phosphate (C7H8NO2+. H2PO4−). *Journal of Molecular Structure* **2021**, *1242*, 130707, https://doi.org/10.1016/j.molstruc.2021.130707.
20. Zerraf, S.; Belhabra, M.; Tridane, M.; Belaaouad, S. Chemical preparation, thermal behavior and IR studies of the New chromium diphosphate hydrate and crystal structure of its corresponding anhydrous. *Biointerface Res. Appl. Chem* **2021**, *11*, 13412-13420, https://doi.org/10.33263/BRIAC115.1341213420.
21. Majdi, E.M.; El Makhloufy, S.; Ouasri, A.; Saadi, M.; El Ammari, L.; Belaaouad, S. Chemical preparation, crystal structure reinvestigation, and vibrational study of meta-carboxyphenyl ammonium dihydrogenomonophosphate (C7H4NH3OOH) H2PO4 (mC AMP). *Molecular Crystals and Liquid Crystals* **2021**, *714*, 14-25, https://doi.org/10.1080/15421406.2020.1848255.
22. Moseley, J; Krasikov, D; Lee, C; Kuciauskas, D. Diverse simulations of time-resolved photoluminescence in thin-film solar cells: A SnO2/CdSeyTe1− y case study. *Journal of Applied Physics* **2021**, *130*, 163105, https://doi.org/10.1063/5.0063028.
23. Doroody, C.; Rahman, K.S.; Kiong, T. S.; Amin, N. Optoelectrical impact of alternative window layer composition in CdTe thin film solar cells perfillance. *Solar Energy* **2022**, *233*, 523-530, https://doi.org/10.1016/j.solener.2022.01.049.
24. Lan, H.; Xiao, H.; Zhao, J., Chen, X.;Fan, P.; Liang, G. All-inorganic CsPbBr3 thin-film solar cells prepared by single-source physical vapor deposition. *Materials Science in Semiconductor Processing* **2021**, *132*, 105869, https://doi.org/10.1016/j.mssp.2021.105869.
25. Gruginskie, N.; Cappelluti, F.; van Eerden, M.; Bauhuis, G.; Mulder, P.; Vlieg, E.; Schermer, J. Proton irradiation induced GaAs solar cell perfillance degradation simulations using a physics-based model. *Solar Energy Materials and Solar Cells* **2021**, *223*, 110971, https://doi.org/10.1016/j.solmat.2021.110971.
26. Goossens, V.M.; Sukharevska, N.V.; Dirin, D.N.; Kovalenko, M.V.; Loi, M.A. Scalable fabrication of efficient pn junction lead sulfide quantum dot solar cells. *Cell Reports Physical Science* **2021**, *2*, 100655, https://doi.org/10.1016/j.xcrp.2021.100655.
27. Shrestha, S.; Li, X.; Tsai, H.; Hou, C.H.; Huang, H.H.; Ghosh, D.; Nie, W. Long carrier diffusion length in two-dimensional lead halide perovskite single crystals. *Chem* **2022**, *8*, 1107-1120, https://doi.org/10.1016/j.chempr.2022.01.008.
28. Huang, L.; Yu, B.; Zhu, F.; Tian, W.; Lian, G.; Zhang, T.; Wong, C.P. Spin-coating thermal-pressed strategy for the preparation of inorganic perovskite quasi-single-crystal thin films with giant single-/two-photon responses. *Nano Energy* **2022**, *92*, 106719, https://doi.org/10.1016/j.nanoen.2021.106719.
29. Gu, J.; Yu, Y.; Chen, S.; Shi, W.; Wang, Y.; Liao, Y.; Jiang, F. Heterojunction photocatalyst of cavity shaped Bi2S3/g-C3N4 for bisphenol a degradation: Regulation of internal electric field via assistance of interfacial functional groups. *Chemical Engineering Journal* **2021**, *424*, 130539, https://doi.org/10.1016/j.cej.2021.130539.
30. De Giorgi, M.L.; Milanese, S.; Klini, A.; Anni, M. Environment-induced reversible modulation of optical and electronic properties of lead halide perovskites and possible applications to sensor development: a review. *Molecules* **2021**, *26*, 705, https://doi.org/10.3390/molecules26030705.

31. Mana-ay, H.; Wang, C.Y.; Hung, K.Y.; Chen, P. Y.; Tu, C. S.; Chen, C. S. Electric field poling effect on the photosensitivity of samarium-doped bismuth ferrite ceramics. *Ceramics International* **2021**, *47*, 12574-12582, https://doi.org/10.1016/j.ceramint.2021.01.116.
32. Degrave, S.; Burgelman, M.; Nollet, P. Modelling of polycrystalline thin film solar cells: new features in SCAPS. *3rd World Conference on Photovoltaic Energy Conversion* **2003**, *1*, 487-490.
33. Cruz, A.G.G.; Solís, M.D., González, L.G.; Torres, J.H.; López, M.L.; Puente, G.C.; Peredo, L.Z. Theoretical study of c-GaN/GaAs single heterojunction solar cells. *Matéria (Rio de Janeiro*) **2017**, *22*, 11887, https://doi.org/10.1590/S1517-707620170004.0221.
34. Azza, M.; Daaif, J.; Salah, M.; Belaaouad, S. Theoretical Aspect of Physical Phenomena in Inorganic Photovoltaic Cells. Electrical Modeling and Numerical Simulation. *E3S Web of Conferences* **2021**, *297*, 01024, https://doi.org/10.1051/e3sconf/202129701024.
35. Azza, M.; Daaif, J.; Aouidate, A.; Belaaouad, S. Automatic solution for solar cell photo-current prediction using machine learning. *E3S Web of Conferences* **2021**, *297,* https://doi.org/10.1051/e3sconf/202129701029.
36. Baeg, K.J.; Binda, M.; Natali, D.; Caironi, M.; Noh, Y.Y. Organic light detectors: photodiodes and phototransistors. *Advanced materials* **2013,** *25*, 4267-4295, https://doi.org/10.1002/adma.201204979.
37. Nozik, A.J. Quantum dot solar cells. *Physica E: Low-dimensional Systems and Nanostructures* **2002**, *14*, 115-120, https://doi.org/10.1016/S1386-9477(02)00374-0.
38. Meng, Q.; Wang, Y.; Zhang, L. Irradiance characteristics and optimization design of a large-scale solar simulator. *Solar Energy* **2011,** *85*, 1758-1767, https://doi.org/10.1016/j.solener.2011.04.014.
39. Kadri, R.; Andrei, H.; Gaubert, J.P.; Ivanovici, T.; Champenois, G.; Andrei, P. Modeling of the photovoltaic cell circuit parameters for optimum connection model and real-time emulator with partial shadow conditions. *Energy* **2012,** *42*, 57-67, https://doi.org/10.1016/j.energy.2011.10.018.
40. El Chaar, L.; Iamont, L.A.; El Zein, N. Review of photovoltaic technologies. *Renewable and sustainable energy reviews* **2011**, *15*, 2165-2175, https://doi.org/10.1016/j.rser.2011.01.004.
41. Paulos, S.; Saugar, J.M.; de Lucio, A.; Fuentes, I.; Mateo, M.; Carmena, D. Comparative performance evaluation of four commercial multiplex real-time PCR assays for the detection of the diarrhoea-causing protozoa Cryptosporidium hominis/parvum, Giardia duodenalis and Entamoeba histolytica. *PLoS One* **2019**, *14*, e0215068, https://doi.org/10.1371/journal.pone.0215068.
42. Khelfaoui, N.; Djafour, A.; Ghenai, C.; Laib, I.; Danoune, M.B.; Gougui, A. Experimental investigation of solar hydrogen production PV/PEM electrolyser performance in the Algerian Sahara regions. *International Journal of Hydrogen Energy* **2021**, *46*, 30524-30538, https://doi.org/10.1016/j.ijhydene.2020.11.193.
43. López, C.S.P.; Frontini, F. Energy efficiency and renewable solar energy integration in heritage historic buildings. *Energy Procedia* **2014**, *48*, 1493-1502, https://doi.org/10.1016/j.egypro.2014.02.169.
44. Momma, K.; Izumi, F. VESTA 3 for three-dimensional visualization of crystal, volumetric and morphology data. *Journal of applied crystallography* **2011**, *44*, 1272-1276, https://doi.org/10.1107/S0021889811038970.
45. Krebs, O.; Voisin, P. Giant optical anisotropy of semiconductor heterostructures with no common atom and the quantum-confined Pockels effect. *Physical review letters* **1996**, *77*, 1829, https://doi.org/10.1103/PhysRevLett.77.1829.
46. Bassam, R.; El Alouani, M.; Maissara, J.; Rachdi, Y.; Jarmouni, N; Chbihi, M.E.M.; Belaaouad, S. Physico-chemical characterization of natural rocks and their valorization on the removal of arsenic from aqueous solution. *Materials Today:Proceedings* **2022**, https://doi.org/10.1016/j.matpr.2021.12.498.
47. Jarmouni, N; Tomaiuolo, M; Gabbani, A; Genovese, D; Pineider, F; Bassam, R; Belaaouad S.; Benmokhtar, S. Low temperature synthesis of ultra-green luminescent colloidal FAPbBr3 perovskite nanocrystals. *Materials Today: Proceedings*, https://doi.org/10.1016/j.matpr.2022.02.562.
48. Barrigón, E.; Heurlin, M.; Bi, Z.; Monemar, B.; Samuelson, L. Synthesis and applications of III–V nanowires. *Chemical reviews***2019**, *119*, 9170-9220, https://doi.org/10.1021/acs.chemrev.9b00075.
49. Majdi, E.M.; El Makhloufy, S.; Chtita, S.; Belaaouad, S. Synthesis, crystal structure, IR, Raman spectroscopy, and DFT computation of metacarboxyphenyl ammonium dihydrogenomonophosphate (C7H4NH3OOH) H2PO4 (mC AMP). *Inorganic and Nano-Metal Chemistry* **2021**, *52*, 633-642, https://doi.org/10.1080/24701556.2021.1946081.
50. Dreike, P.L.; Fleetwood, D.M.; King, D.B.; Sprauer, D.C.; Zipperian, T.E. An overview of high-temperature electronic device technologies and potential applications.*IEEE Transactions on Components, Packaging, and Manufacturing Technology: Part A* **1994**, *17*, 594-609, https://doi.org/10.1109/95.335047.
51. Blakemore, J.S. Semiconducting and other major properties of gallium arsenide. *Journal of Applied Physics* **1982**, *53*, R123-R181, https://doi.org/10.1063/1.331665.

52. Yan, X.; Gong, L; Ai, L.; Wei, W.; Zhang, X.; Ren, X. Enhanced photovoltaic performance of nanowire array solar cells with multiple diameters. *Optics Express* **2018,** *26*, A974-A983, https://doi.org/10.1364/OE.26.00A974.